

1 **Technical note: LA–ICP–MS U–Pb dating of unetched and etched apatites**

2 *Fanis Abdullin et al.: LA–ICP–MS U–Pb dating of apatites*

3 Fanis Abdullin¹, Luigi A. Solari², Jesús Solé³, Carlos Ortega-Obregón²

4 ¹CONACyT–Centro de Geociencias, Campus Juriquilla, UNAM, Querétaro, 76230, Mexico

5 ²Centro de Geociencias, Campus Juriquilla, UNAM, Querétaro, 76230, Mexico

6 ³LANGEM, Instituto de Geología, UNAM, Ciudad Universitaria, CDMX, 04510, Mexico

7 **Correspondence:** Fanis Abdullin (fanis@geociencias.unam.mx)

8

9 **Abstract**

10 The same unetched and chemically etched apatite crystals from five rock samples were dated by
11 the U–Pb method via laser ablation inductively-coupled plasma mass spectrometry (LA–ICP–
12 MS). The objective of this study is to test whether chemical etching required for apatite fission
13 track analysis impacts the precision and accuracy of apatite U–Pb geochronology. The results of
14 this experiment suggest that etching has insignificant effects on the accuracy of apatite U–Pb
15 ages obtained by LA–ICP–MS. Therefore, LA–ICP–MS is reliable for U–Pb analysis as part of
16 apatite fission track and U–Pb double dating.

17

18

19 **Short summary**

20 Unetched and etched apatite grains from five samples were dated by U–Pb method using laser
21 ablation inductively-coupled plasma mass spectrometry. Our experiment indicates that etching
22 needed for apatite fission track dating has insignificant effects on obtaining accurate U–Pb ages;

23 thus, the laser ablation-based technique may be used for apatite fission track and U–Pb double
24 dating.

25

26 **1 Introduction**

27

28 Apatite, $\text{Ca}_5(\text{PO}_4)_3[\text{F},\text{Cl},\text{OH}]$, is the most common phosphate mineral in the Earth’s crust and can
29 be found in practically all igneous and metamorphic rocks, in many ancient and recent sediments
30 as well as in certain mineral deposits (Piccoli and Candela, 2002; Morton and Yaxley, 2007;
31 Webster and Piccoli, 2015). This accessory mineral is often used as a natural thermochronometer
32 for fission track, helium, U–Th and U–Pb dating (e.g., Zeitler et al., 1987; Wolf et al., 1996;
33 Ehlers and Farley, 2003; Hasebe et al., 2004; Donelick et al., 2005; Chew and Donelick, 2012;
34 Chew et al., 2014; Cochran et al., 2014; Liu et al., 2014; Spikings et al., 2015; Glorie et al.,
35 2017). Presently, apatite fission track (AFT) ages can be obtained rapidly by using laser ablation
36 inductively-coupled plasma mass spectrometry (LA–ICP–MS) for direct measurement of “parent
37 nuclides”, i.e., ^{238}U contents (Cox et al., 2000; Svojtka and Košler, 2002; Hasebe et al., 2004,
38 2009; Donelick et al., 2005; Abdullin et al., 2014, 2016, 2018; Vermeesch, 2017). The LA–ICP–
39 MS technique may be used to measure ^{238}U for AFT dating, together with Pb isotopes needed for
40 U–Pb dating (e.g., Chew and Donelick, 2012; Liu et al., 2014; Glorie et al., 2017; Bonilla et al.,
41 2020; Nieto-Samaniego et al., 2020).

42 Hasebe et al. (2009) previously performed an important experimental study, during which
43 they demonstrated that chemical etching required for apatite/zircon fission track dating does not
44 interfere with U analysis by LA–ICP–MS. The influence of etching needed for AFT dating on the
45 precision and accuracy of dating the same crystals by U–Pb using LA–ICP–MS remains to be

46 quantified. To investigate this issue, the same unetched and etched apatite grains extracted from
47 five rock samples were analyzed via LA-ICP-MS for U-Pb dating. The chosen samples have
48 either emplacement or metamorphic ages ranging from the Cretaceous to the Neoproterozoic (see
49 Table 1 for further details).

50 --- **Table 1** ---

51

52

53 **2 Sample descriptions**

54

55 2.1 OV-0421 (Tres Sabanas Pluton, Guatemala)

56

57 This sample is a two mica-bearing deformed granite belonging to the Tres Sabanas Pluton, which
58 is located northwest of Guatemala City, Guatemala. For sample OV-0421, an emplacement age
59 of 115 ± 4 (2σ) Ma was proposed based on zircon U-Pb data (Torres de León, 2016). A cooling
60 age of 102 ± 1 (2σ) Ma, obtained with K-Ar (on biotite), was also reported by the same author.

61

62 2.2. MCH-38 (Chiapas Massif Complex, Mexico)

63

64 MCH-38 is an orthogneiss from the Permian Chiapas Massif Complex. This rock was sampled to
65 the west of Unión Agrarista, the State of Chiapas, southeastern Mexico. There is no reported age
66 for this sample. Some zircon U-Pb dates obtained for the Chiapas Massif Complex (Weber et al.,
67 2007, 2008; Ortega-Obregón et al., 2019) suggest that a Lopingian (260–252 Ma) crystallization
68 or metamorphic age may be assumed for sample MCH-38.

69

70 2.3 TO-AM (Totoltepec Pluton, Mexico)

71

72 TO-AM is a granitic rock, sampled ca. 5 km west of Totoltepec de Guerrero, the State of Puebla,
73 southern Mexico. There is no reported radiometric data for sample TO-AM. Previous geological
74 studies indicate that the Pennsylvanian–Cisuralian Totoltepec Pluton was emplaced over a ca. 23
75 million year period (from ca. 308 to ca. 285 Ma; e.g., Kirsch et al., 2013).

76

77 2.4 CH-0403 (Altos Cuchumatanes, Guatemala)

78

79 CH-0403 was collected 5 km ESE of Barillas, in the Altos Cuchumatanes, Guatemala. It consists
80 of a gray to green granodiorite. Five zircon aliquots of sample CH-0403 were dated using isotope
81 dilution thermal-ionization mass spectrometry, yielding a lower intercept date of 391 ± 8 (2σ)
82 Ma that is interpreted as its approximate crystallization age (Solari et al., 2009).

83

84 2.5 OC-1008 (Oaxacan Complex, Mexico)

85

86 This sample is a paragneiss from the Grenvillian Oaxacan Complex, southern Mexico. OC-1008
87 was collected in the federal road which connects Nochixtlán to Oaxaca. It was demonstrated that
88 this sample underwent granulite facies metamorphism at 1000–980 Ma (Solari et al., 2014).

89

90

91

92 3 Analytical procedures

93
94 Accessory minerals were concentrated using conventional mineral separation techniques such as
95 rock crushing, sieving, Wilfley table, Frantz magnetic separator, and bromoform. Approximately
96 300 apatite grains were extracted from each rock sample and mounted with their surfaces parallel
97 to the crystallographic *c*-axis in a 2.5 cm diameter epoxy mount. Mounted crystals were polished
98 to expose their internal surfaces (i.e., up to 4π geometry). For this experiment, complete crystals
99 lacking visible inclusions and other defects, such as cracks, were carefully selected for analysis.
100 Sample preparation was performed at Taller de Molienda and Taller de Laminación, Centro de
101 Geociencias (CGEO), Campus Juriquilla, Universidad Nacional Autónoma de Mexico (UNAM).

102 Single spot analyses were performed with a Resonetics RESolution™ LPX Pro (193 nm,
103 ArF excimer) laser ablation system, coupled to a Thermo Scientific iCAP™ Qc quadrupole ICP-
104 MS at Laboratorio de Estudios Isotópicos (LEI), CGEO, UNAM. During this experimental work,
105 LA–ICP-MS-based sampling was performed in central parts of the selected apatite grains before
106 and after chemical etching (in 5.5M HNO₃ at 21 °C for 20 s to reveal spontaneous fission tracks),
107 as shown schematically in Fig. 1. The LA–ICP-MS protocol used for apatite analyses, as given in
108 Table 2, was established on the basis of numerous experiments carried out at LEI during the past
109 five years, and can be used for U–Pb and fission track double dating plus multielemental analysis
110 (Abdullin et al., 2018; Ortega-Obregón et al., 2019). Corrected isotopic ratios and errors were
111 calculated using Iolite 3.5 (Paton et al., 2011) and the VizualAge data reduction scheme (Petrus
112 and Kamber, 2012). UcomPbine (Chew et al., 2014) was used to model ²⁰⁷Pb/²⁰⁶Pb initial values
113 and thus force a ²⁰⁷Pb correction that considers the common Pb (non-radiogenic Pb) incorporated
114 by apatite standards at the moment of their crystallization (see also Ortega-Obregón et al., 2019).

115 The “First Mine Discovery” apatite from Madagascar, with a mean U–Pb age of ca. 480 Ma
116 (Thomson et al., 2012; Chew et al., 2014), was used as a primary reference material. The results
117 for measured isotopes using NIST-612 (Pearce et al., 1997) were normalized using ^{43}Ca as an
118 internal standard and taking an average CaO content of 55%.

119 Tera–Wasserburg Concordia diagrams (T–W; Tera and Wasserburg, 1972) are used in
120 apatite U–Pb dating, because the LA–ICP–MS-derived U–Pb results are generally discordant.
121 The lower intercept in the T–W plot is considered as a mean apatite U–Pb age that should have
122 geological significance (crystallization or cooling age, the age of mineralization or metamorphic
123 event). Apatite U–Pb ages were calculated with IsoplotR (Vermeesch, 2017, 2018) and described
124 below. Detailed information on U–Pb experiments is given in Table S1 in the Supplement.

125 --- **Figure 1** ---

126 --- **Table 2** ---

127

128

129 **4 Results**

130

131 4.1 OV-0421

132

133 For rock sample OV-0421, 41 unetched apatites yielded a lower intercept age of 106 ± 4 (2σ) Ma
134 with a mean square weighted deviation (MSWD) of 1.07, passing the chi-squared test with the
135 $P(\chi^2)$ value of 0.35 (see in Fig. 2). Practically the same U–Pb date, 107 ± 5 (2σ) Ma, was
136 obtained after chemical etching of the same apatite grains, yielding a MSWD of 1.13 and a $P(\chi^2)$
137 of 0.27. Both these apatite U–Pb ages lie between the zircon U–Pb date of 115 ± 4 (2σ) Ma (i.e.,

138 crystallization age) and the biotite K–Ar age of 102 ± 1 (2σ) Ma (i.e., cooling age), which were
139 previously obtained for the same granite sample by Torres de León (2016).

140

141 4.2. MCH-38

142

143 For orthogneiss sample MCH-38, the lower intercept in T–W yielded a U–Pb age of 245 ± 6 (2σ)
144 Ma (obtained from 41 unetched apatites) with a MSWD of 0.28 and a $P(\chi^2)$ of 1. Etched apatite
145 grains from MCH-38 yielded an age of 240 ± 4 (2σ) Ma with a MSWD of 0.36 and a $P(\chi^2)$ of 1
146 (Fig. 2). Our U–Pb results are in close agreement with geochronological data reported from the
147 Chiapas Massif Complex in previous studies (Damon et al., 1981; Torres et al., 1999; Schaaf et
148 al., 2002; Ortega-Obregón et al., 2019). For instance, Torres et al. (1999) compiled biotite K–Ar
149 ages, most of which lie within Early–Middle Triassic period. Triassic cooling ages in the Chiapas
150 Massif Complex were also detected by Rb–Sr in mica–whole rock pairs that range from 244 ± 12
151 (2σ) Ma to 214 ± 11 (2σ) Ma (Schaaf et al., 2002).

152

153 4.3 TO-AM

154

155 Unetched apatites (32 crystals; Fig. 2) from granite TO-AM yielded a lower intercept date of 303
156 ± 5 (2σ) Ma with a MSWD of 0.6 and a $P(\chi^2)$ of 0.96. After etching, a slightly younger age of
157 299 ± 3 (2σ) Ma was obtained, with a MSWD of 0.89 and a $P(\chi^2)$ of 0.65. These apatite U–Pb
158 ages are in line with the zircon U–Pb ages of 306 ± 2 (2σ) Ma to 287 ± 2 (2σ) Ma reported for
159 the Pennsylvanian–Cisuralian Totoltepec Pluton (e.g., see details in Kirsch et al., 2013).

160

161 4.4 CH-0403

162

163 36 unetched apatite grains from sample CH-0403 yielded a lower intercept U–Pb age of 345 ± 10
164 (2σ) Ma with a MSWD of 0.7 and a $P(\chi^2)$ of 0.9, whereas etched grains yielded an age of 334 ± 8
165 (2σ) Ma with a MSWD of 1.37 and a $P(\chi^2)$ of 0.08 (Fig. 2). These cooling dates are considerably
166 younger if compared to the CH-0403 emplacement age of 391 ± 8 (2σ) Ma (Solari et al., 2009).

167

168 4.5 OC-1008

169

170 41 unetched apatites belonging to sample OC-1008 yielded a U–Pb age of 839 ± 12 (2σ) Ma with
171 a MSWD of 0.98 and a $P(\chi^2)$ of 0.50. After etching, the same apatite crystals yielded an age of
172 830 ± 10 (2σ) Ma with a MSWD of 1.24 and a $P(\chi^2)$ of 0.14 (Fig. 2). Both these apatite U–Pb
173 ages are significantly younger than the age of granulite facies metamorphism in the Grenville-
174 aged Oaxacan Complex (1 Ga to 980 Ma, Solari et al., 2014), and thus, should be considered as
175 cooling ages.

176

--- Figure 2 ---

177

178

179 **5 Discussion and concluding remarks**

180

181 Most rock samples, except OV-0421, yielded slightly younger apatite U–Pb ages after chemical
182 etching (up to 3.3% in sample CH-0403). However, the lower intercept U–Pb ages obtained from
183 unetched apatite grains are indistinguishable within error from the U–Pb ages obtained on the

184 same etched grains (see diagram in Fig. 3). The results of this experiment demonstrate that
185 chemical etching required for AFT analysis has negligible effects on the accuracy of apatite U–
186 Pb ages determined via LA–ICP-MS. Thus, as a main conclusion of this study, LA–ICP-MS can
187 be used for simultaneous AFT and U–Pb double dating, as it was already done in some previous
188 studies (e.g., Chew and Donelick, 2012; Liu et al., 2014; Glorie et al., 2017; Bonilla et al., 2020;
189 Nieto-Samaniego et al., 2020).

190 --- **Figure 3** ---

191

192 **Supplement**

193 The supplement related to this article is available online at: <https://...>

194

195 **Author contributions**

196 Conceptualisation, investigation, and writing of the original draft were done by FA. LS and COO
197 provided technical support. LS and JS acquired funding and resources, supervised the study, and
198 reviewed the manuscript.

199

200 **Competing interests**

201 The authors declare that they have no conflict of interest.

202

203

204 **Acknowledgements**

205 The authors are grateful to Juan Tomás Vázquez Ramírez and Ofelia Pérez Arvizu for their help
206 with sample preparation for this study. Professor Stuart Thomson is acknowledged for sharing

207 Madagascar apatite. Dr. Michelangelo Martini kindly provided sample TO-AM that was useful
208 for our experimental study. Dr. Ziva Shulaker, Dr. Jakub Sliwinski, and Professor Axel Schmitt
209 are acknowledged for their constructive comments that improved our manuscript significantly.

210

211 **Financial support**

212 This research has been supported by PAPIIT DGAPA UNAM (grant no. IN101520 to LS).

213

214

215 **Figure caption**

216

217 **Figure 1**

218 Illustration displaying the LA-ICP-MS-based U-Pb dating of the same apatite crystal before and
219 after chemical etching (i.e., etched in 5.5M nitric acid at 21 °C for 20 s). Spot diameter of 60 µm.

220

221 **Figure 2**

222 Tera-Wasserburg Concordia diagrams for the U-Pb results of unetched and etched apatites from
223 samples OV-0421, MCH-38, TO-AM, CH-0403, and OC-1008. MSWD – mean square weighted
224 deviation, Ngr – number of grains dated. Errors are given in 2σ .

225

226 **Figure 3**

227 Plot showing the lower intercept U-Pb ages obtained on unetched and etched apatite grains.

228

229

230 **References**

231

232 Abdullin, F., Solé, J., and Solari, L.: Datación mediante trazas de fisión y análisis multielemental
233 con LA-ICP-MS del fluorapatito de Cerro de Mercado (Durango, México), *Revista Mexicana de*
234 *Ciencias Geológicas*, 31, 395–406, 2014.

235

236 Abdullin, F., Solé, J., Meneses-Rocha, J.D.J., Solari, L., Shchepetilnikova, V., and Ortega-
237 Obregón, C.: LA-ICP-MS-based apatite fission track dating of the Todos Santos Formation
238 sandstones from the Sierra de Chiapas (SE Mexico) and its tectonic significance, *International*
239 *Geology Review*, 58, 32–48, 2016,
240 <https://doi.org/10.1080/00206814.2015.1055596>.

241

242 Abdullin, F., Solari, L., Ortega-Obregón, C., and Solé, J.: New fission-track results from the
243 northern Chiapas Massif area, SE Mexico: trying to reconstruct its complex thermo-tectonic
244 history, *Revista Mexicana de Ciencias Geológicas*, 35, 79–92,
245 <https://doi.org/10.22201/cgeo.20072902e.2018.1.523>, 2018.

246

247 Bonilla, A., Franco, J. A., Cramer, T., Poujol, M., Cogné, N., Nachtergaele, S., and De Grave, J.:
248 Apatite LA-ICP-MS U–Pb and fission-track geochronology of the Caño Viejita gabbro in E-
249 Colombia: Evidence for Grenvillian intraplate rifting and Jurassic exhumation in the NW
250 Amazonian Craton, *Journal of South American Earth Sciences*, 98, 102438,
251 <https://doi.org/10.1016/j.jsames.2019.102438>, 2020.

252

253 Chew, D. M., and Donelick, R. A.: Combined apatite fission track and U-Pb dating by LA-ICP-
254 MS and its application in apatite provenance analysis, *Quantitative Mineralogy and*
255 *Microanalysis of Sediments and Sedimentary Rocks: Mineralogical Association of Canada,*
256 *Short Course, 42, 219–247, 2012.*

257

258 Chew, D. M., Petrus, J. A., and Kamber, B. S.: U–Pb LA–ICPMS dating using accessory mineral
259 standards with variable common Pb, *Chemical Geology, 363, 185–199,*
260 <https://doi.org/10.1016/j.chemgeo.2013.11.006>, 2014.

261

262 Cochrane, R., Spikings, R. A., Chew, D., Wotzlaw, J. F., Chiaradia, M., Tyrrell, S., Schaltegger,
263 U., and Van der Lelij, R.: High temperature (> 350 °C) thermochronology and mechanisms of Pb
264 loss in apatite, *Geochimica et Cosmochimica Acta, 127, 39–56,*
265 <https://doi.org/10.1016/j.gca.2013.11.028>, 2014.

266

267 Cox, R., Košler, J., Sylvester, P., and Hodych, P.: Apatite fission-track (FT) dating by LAM-
268 ICP-MS analysis, Goldschmidt Conference, Oxford, UK, *Journal of Conference Abstracts, 5, p.*
269 *322, 2000.*

270

271 Damon, P. E., Shafiqullah, M., and Clark, K. F.: Age trends of igneous activity in relation to
272 metallogenesis in the southern Cordillera, Tucson, Arizona, *Arizona Geological Society Digest,*
273 *14, 137–153, 1981.*

274

275 Donelick, R. A., O’Sullivan, P. B., and Ketcham, R. A.: Apatite fission-track analysis, *Reviews*
276 *in Mineralogy and Geochemistry*, 58, 49–94, <https://doi.org/10.2138/rmg.2005.58.3>, 2005.
277

278 Ehlers, T. A., and Farley, K. A.: Apatite (U–Th)/He thermochronometry: methods and
279 applications to problems in tectonic and surface processes, *Earth and Planetary Science Letters*,
280 206, 1–14, [https://doi.org/10.1016/S0012-821X\(02\)01069-5](https://doi.org/10.1016/S0012-821X(02)01069-5), 2003.
281

282 Glorie, S., Alexandrov, I., Nixon, A., Jepson, G., Gillespie, J., and Jahn, B. M.: Thermal and
283 exhumation history of Sakhalin Island (Russia) constrained by apatite U-Pb and fission track
284 thermochronology, *Journal of Asian Earth Sciences*, 143, 326–342,
285 <https://doi.org/10.1016/j.jseaes.2017.05.011>, 2017.
286

287 Hasebe, N., Barbarand, J., Jarvis, K., Carter, A., and Hurford, A. J.: Apatite fission-track
288 chronometry using laser ablation ICP-MS, *Chemical Geology*, 207, 135–145,
289 <https://doi.org/10.1016/j.chemgeo.2004.01.007>, 2004.
290

291 Hasebe, N., Carter, A., Hurford, A. J., and Arai, S.: The effect of chemical etching on LA–ICP-
292 MS analysis in determining uranium concentration for fission-track chronometry, *Geological*
293 *Society, London, Special Publications*, 324, 37–46, <https://doi.org/10.1144/SP324.3>, 2009.
294

295 Kirsch, M., Keppie, J. D., Murphy, J. B., and Lee, J. K.: Arc plutonism in a transtensional
296 regime: the late Palaeozoic Totoltepec pluton, Acatlán Complex, southern Mexico, *International*
297 *Geology Review*, 55, 263–286, <https://doi.org/10.1080/00206814.2012.693247>, 2013.

298

299 Liu, W., Zhang, J., Sun, T., Wang, J.: Application of apatite U–Pb and fission-track double
300 dating to determine the preservation potential of magnetite–apatite deposits in the Luzong and
301 Ningwu volcanic basins, eastern China, *Journal of Geochemical Exploration*, 138, 22–32,
302 <https://doi.org/10.1016/j.gexplo.2013.12.006>, 2014.

303

304 Morton, A., and Yaxley, G.: Detrital apatite geochemistry and its application in provenance
305 studies, *Special Papers, Geological Society of America*, 420, 319,
306 [https://doi.org/10.1130/2006.2420\(19\)](https://doi.org/10.1130/2006.2420(19)), 2007.

307

308 Nieto-Samaniego, A. F., Olmos-Moya, M. D. J. P., Levresse, G., Alaniz-Alvarez, S. A.,
309 Abdullin, F., del Pilar-Martínez, A., and Xu, S.: Thermochronology and exhumation rates of
310 granitic intrusions at Mesa Central, Mexico, *International Geology Review*, 62, 311–319,
311 <https://doi.org/10.1080/00206814.2019.1602789>, 2020.

312

313 Ortega-Obregón, C., Abdullin, F., Solari, L., Schaaf, P., and Solís-Pichardo, G.: Apatite U-Pb
314 dating at UNAM laboratories: analytical protocols and examples of its application, *Revista
315 Mexicana de Ciencias Geológicas*, 36, 27–37,
316 <https://doi.org/10.22201/cgeo.20072902e.2019.1.749>, 2019.

317

318 Paton, C., Hellstrom, J., Paul, B., Woodhead, J., Hergt, J.: Iolite: Freeware for the visualisation
319 and processing of mass spectrometric data, *Journal of Analytical Atomic Spectrometry*, 26,
320 2508–2518, <https://doi.org/10.1039/C1JA10172B>, 2011.

321
322 Pearce, N. J., Perkins, W. T., Westgate, J. A., Gorton, M. P., Jackson, S. E., Neal, C. R., and
323 Chenery, S. P.: A compilation of new and published major and trace element data for NIST SRM
324 610 and NIST SRM 612 glass reference materials, *Geostandards newsletter*, 21, 115–144,
325 <https://doi.org/10.1111/j.1751-908X.1997.tb00538.x>, 1997.
326
327 Petrus, J. A., and Kamber, B. S.: VizualAge: A novel approach to laser ablation ICP-MS U-Pb
328 geochronology data reduction, *Geostandards and Geoanalytical Research*, 36, 247–270,
329 <https://doi.org/10.1111/j.1751-908X.2012.00158.x>, 2012.
330
331 Piccoli, P. M., and Candela, P. A.: Apatite in igneous systems, *Reviews in Mineralogy and*
332 *Geochemistry*, 48, 255–292, <https://doi.org/10.2138/rmg.2002.48.6>, 2002.
333
334 Schaaf, P., Weber, B., Weis, P., Groß, A., Ortega-Gutiérrez, F., and Kohler, H.: The Chiapas
335 Massif (Mexico) revised: New geologic and isotopic data and basement characteristics, *Neues*
336 *Jahrbuch für Geologie und Paläontologie, Abhandlungen*, 225, 1–23, 2002.
337
338 Solari, L. A., Ortega-Gutiérrez, F., Elías-Herrera, M., Schaaf, P., Norman, M., Ortega-Obregón,
339 C., and Chiquín, M.: U-Pb zircon geochronology of Palaeozoic units in western and central
340 Guatemala: Insights into the tectonic evolution of Middle America, *Geological Society, London,*
341 *Special Publications*, 328, 295–313, <https://doi.org/10.1144/SP328.12>, 2009.
342

343 Solari, L. A., Ortega-Gutiérrez, F., Elías-Herrera, M., Ortega-Obregón, C., Macías-Romo, C.,
344 Reyes-Salas, M.: Detrital provenance of the Grenvillian Oaxacan Complex, southern Mexico: a
345 zircon perspective, *International Journal of Earth Sciences*, 103, 1301–1315,
346 <https://doi.org/10.1007/s00531-013-0938-9>, 2014.

347

348 Spikings, R., Cochrane, R., Villagomez, D., Van der Lelij, R., Vallejo, C., Winkler, W., and
349 Beate, B.: The geological history of northwestern South America: From Pangaea to the early
350 collision of the Caribbean large igneous province (290–75 Ma), *Gondwana Research*, 27, 95–
351 139, <https://doi.org/10.1016/j.gr.2014.06.004>, 2015.

352

353 Svojtka, M., and Košler: Fission-track dating of zircon by LA-ICP-MS, Goldschmidt
354 Conference, Davos, Switzerland, *Journal of Conference Abstracts, Special Supplement of*
355 *Geochimica et Cosmochimica Acta*, 66, A756, 2002.

356

357 Tera, F., and Wasserburg, G. J.: U-Th-Pb systematics in three Apollo 14 basalts and the problem
358 of initial Pb in lunar rocks, *Earth and Planetary Science Letters*, 14, 281–304,
359 [https://doi.org/10.1016/0012-821X\(72\)90128-8](https://doi.org/10.1016/0012-821X(72)90128-8), 1972.

360

361 Thomson, S. N., Gehrels, G. E., Ruiz, J., and Buchwaldt, R.: Routine low-damage apatite U-Pb
362 dating using laser ablation–multicollector–ICPMS, *Geochemistry, Geophysics, Geosystems*,
363 13(2), <https://doi.org/10.1029/2011GC003928>, 2012.

364

365 Torres, R., Ruiz, J., Patchett, P. J., Grajales, J. M., Bartolini, C., Wilson, J. L., and Lawton, T. F.:
366 Permo-Triassic continental arc in eastern Mexico: Tectonic implications for reconstruction of
367 southern North America, , Geological Society of America, Special Papers, 340, 191–196,
368 <https://doi.org/10.1130/0-8137-2340-X.191>, 1999.

369

370 Torres de León, R.: Caracterización geológica y geocronológica de unidades metamórficas e
371 intrusivas de la región centro–Oeste de la Cuenca del Rio Motagua, Sureste de Guatemala,
372 Centroamerica: implicaciones en las conexiones Sur de México–Bloque Chortís, Universidad
373 Nacional Autónoma de México, Posgrado en Ciencias de la Tierra, Ph.D Thesis, 221 pp., 2016.

374

375 Vermeesch, P.: Statistics for LA-ICP-MS based fission track dating, *Chemical Geology*, 456,
376 19–27, <https://doi.org/10.1016/j.chemgeo.2017.03.002>, 2017.

377

378 Vermeesch, P.: IsoplotR: A free and open toolbox for geochronology, *Geoscience Frontiers*, 9,
379 1479–1493, <https://doi.org/10.1016/j.gsf.2018.04.001>, 2018.

380

381 Weber, B., Iriondo, A., Premo, W. R., Hecht, L., and Schaaf, P.: New insights into the history
382 and origin of the southern Maya block, SE Mexico: U–Pb–SHRIMP zircon geochronology from
383 metamorphic rocks of the Chiapas massif, *International Journal of Earth Sciences*, 96, 253–269,
384 <https://doi.org/10.1007/s00531-006-0093-7>, 2007.

385

386 Weber, B., Valencia, V. A., Schaaf, P., Pompa-Mera, V., and Ruiz, J.: Significance of
387 provenance ages from the Chiapas Massif Complex (southeastern Mexico): redefining the

388 Paleozoic basement of the Maya Block and its evolution in a peri-Gondwanan realm, *The*
389 *Journal of Geology*, 116, 619–639, <https://doi.org/10.1086/591994>, 2008.

390

391 Webster, J. D., and Piccoli, P. M.: Magmatic apatite: A powerful, yet deceptive, mineral,
392 *Elements*, 11, 177–182, <https://doi.org/10.2113/gselements.11.3.177>, 2015.

393

394 Wolf, R. A., Farley, K. A., and Silver, L. T.: Helium diffusion and low-temperature
395 thermochronometry of apatite, *Geochimica et Cosmochimica Acta*, 60, 4231–4240,
396 [https://doi.org/10.1016/S0016-7037\(96\)00192-5](https://doi.org/10.1016/S0016-7037(96)00192-5), 1996.

397

398 Zeitler, P. K., Herczeg, A. L., McDougall, I., and Honda, M.: U-Th-He dating of apatite: A
399 potential thermochronometer, *Geochimica et Cosmochimica Acta*, 51, 2865–2868,
400 [https://doi.org/10.1016/0016-7037\(87\)90164-5](https://doi.org/10.1016/0016-7037(87)90164-5), 1987.

401

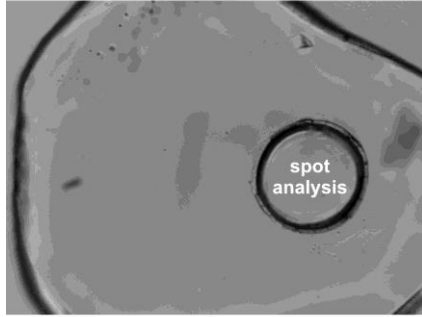
402

403

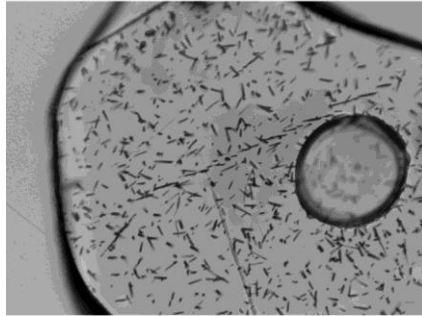
404

Figure 1

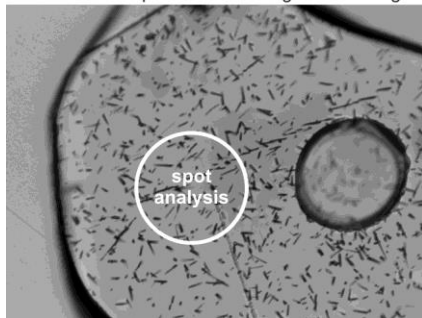
LA-ICP-MS apatite U-Pb dating before etching



chemical etching (5.5M nitric acid, 21 °C for 20 s)



LA-ICP-MS apatite U-Pb dating after etching



405

406

407

408

409

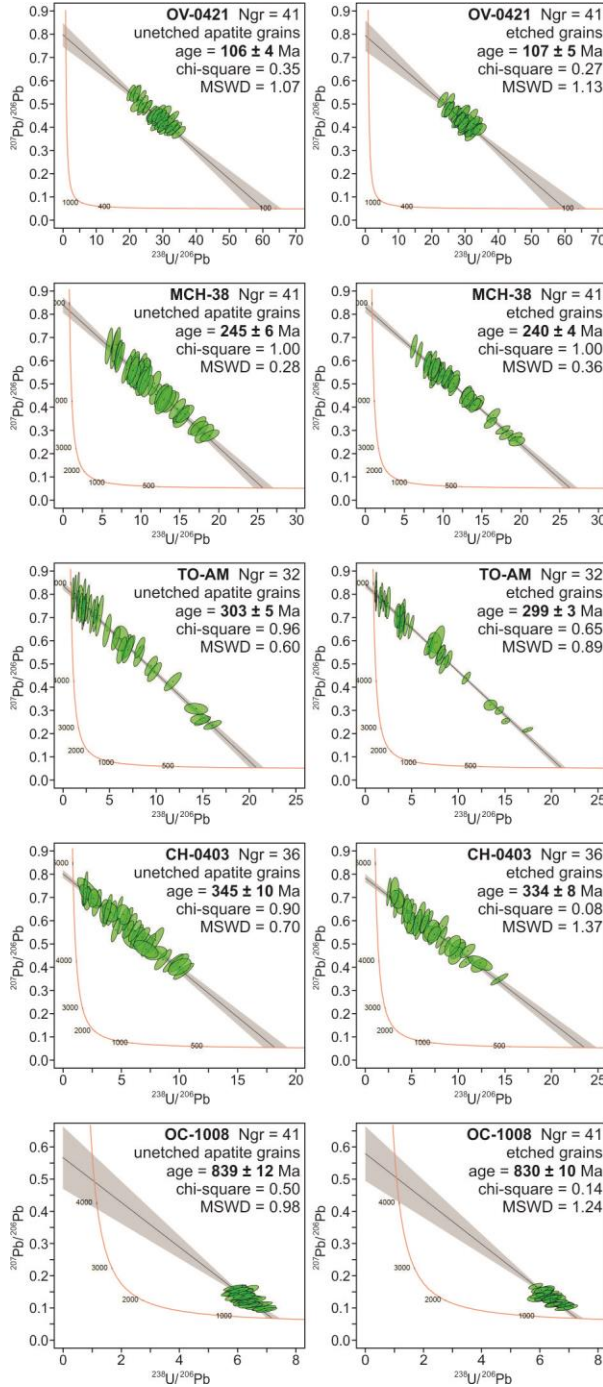
410

411

412

413

Figure 2



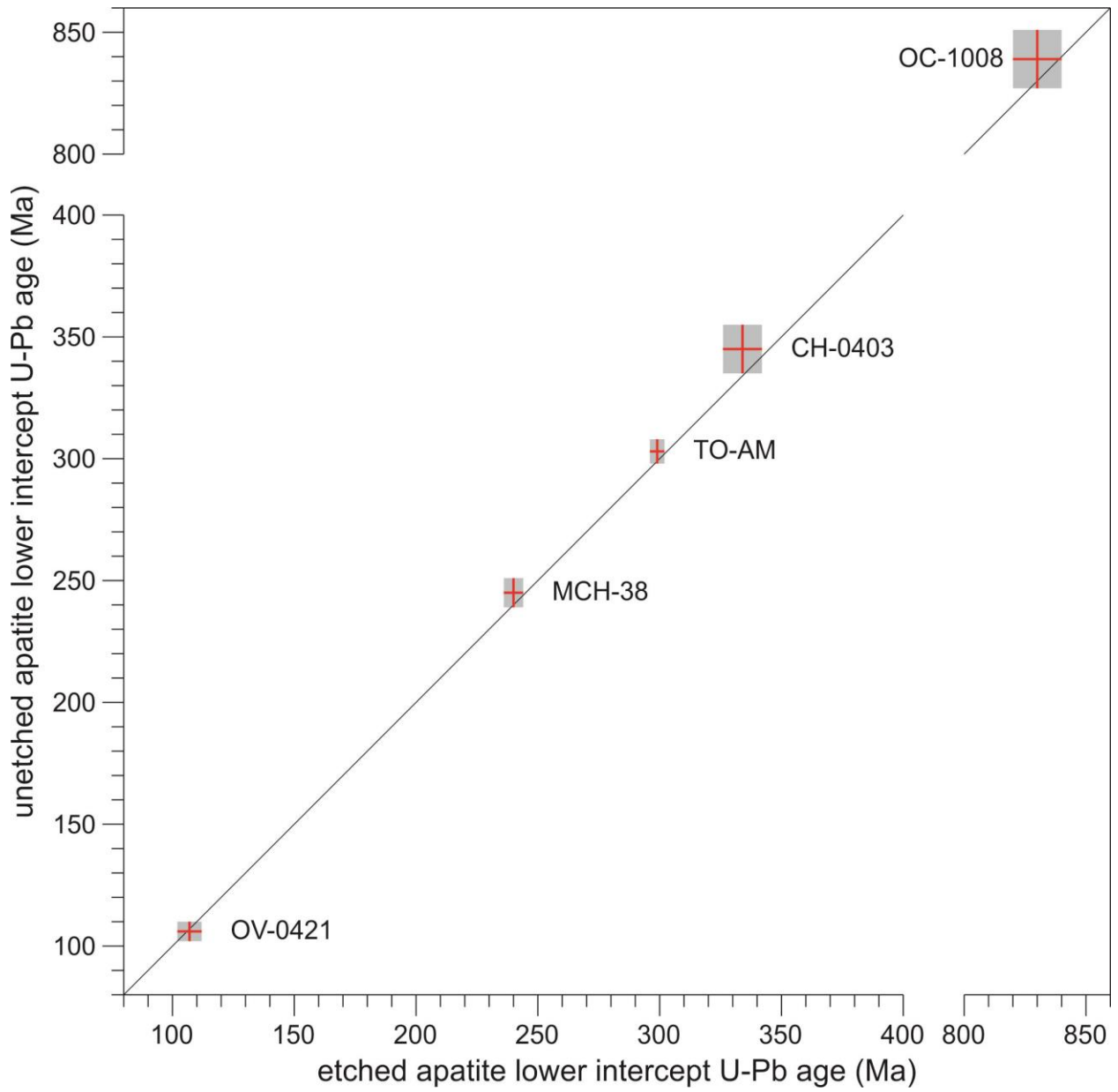
415

416

417

418

Figure 3



420

421

422

423

424

425

426

427 **Table 1**

428

429 Lithology, locality, and zircon U–Pb data for the selected experimental rock samples.

Sample	Unit and locality	Rock type	Zircon U–Pb age	References
OV-0421	Tres Sabanas Pluton, Guatemala	deformed granite	115 ± 4 Ma	Torres de León (2016)
MCH-38	Chiapas Massif Complex, Mexico	orthogneiss	ca. 260 to ca. 252 Ma (?)	Weber et al. (2007, 2008)
TO-AM	Totoltepec Pluton, Mexico	granite	ca. 308 to ca. 285 Ma (?)	Kirsch et al. (2013)
CH-0403	Altos Cuchumatanes, Guatemala	granodiorite	391 ± 8 Ma	Solari et al. (2009)
OC-1008	Oaxacan Complex, Mexico	paragneiss	990 ± 10 Ma	Solari et al. (2014)

430

431

432

433

434

435

436

437

438

439

440

441

442

443

444

445

446 **Table 2**

447

448 LA-ICP-MS protocol established at LEI to be applied for simultaneous apatite U-Pb and fission-
 449 track double dating plus multielemental analysis (REEs, Y, Sr, Mn, Mg, Th, U, and Cl).

<i>ICP-MS operating conditions</i>	
Instrument	Thermo Scientific™ iCAP™ Qc
Forward power	1450 W
Carrier gas flow rate	~1 L/min (Ar) and ~0.35 L/min (He)
Auxiliary gas flow rate	~1 L/min
Plasma gas flow rate	~14 L/min
Nitrogen	~3.5 mL/min
<i>Data acquisition parameters</i>	
Mode of operating	STD (standard mode)
Sampling scheme	-2NIST-612-2MAD-1DUR-10apt-
Background scanning	15 s
Data acquisition time	35 s
Wash-out time	15 s
Measured isotopes	²⁶ Mg ³¹ P ³⁵ Cl ⁴³ Ca ⁴⁴ Ca ⁵⁵ Mn ⁸⁸ Sr ⁸⁹ Y ¹³⁹ La ¹⁴⁰ Ce ¹⁴¹ Pr ¹⁴⁶ Nd ¹⁴⁷ Sm ¹⁵³ Eu ¹⁵⁷ Gd ¹⁵⁹ Tb ¹⁶³ Dy ¹⁶⁵ Ho ¹⁶⁶ Er ¹⁶⁹ Tm ¹⁷² Yb ¹⁷⁵ Lu ²⁰² Hg ²⁰⁴ Pb ²⁰⁶ Pb ²⁰⁷ Pb ²⁰⁸ Pb ²³² Th ²³⁸ U [total = 29]
<i>Laser ablation system</i>	
Ablation cell	RESolution™ Laurin Technic S-155
Model of laser	Resonetics RESolution™ LPX Pro
Wavelength	193 nm (Excimer ArF)
Repetition rate	4 Hz
Energy density	*4 J/cm ²
Mode of sampling	spot diameter of 60 μm

450

451 Note: MAD – “First mine Discovery” U-Pb apatite standard from Madagascar; DUR – Durango
 452 apatite from Cerro de Mercado mine (Mexico); apt – unknown apatite crystals. (*) Laser pulse
 453 energy of 4 J/cm², which was measured directly on target with a Coherent™ laser energy meter.